PARAMETRIC STUDY OF THE SLIP DISTRIBUTION ON THE VERTICAL STRIKE-SLIP FAULT FOR DIFFERENT SOURCE PARAMETERS BASED ON THE DYNAMIC RUPTURE SIMULATION

A. MANPO[1], A. PITARKA[2], H. KAWASE[1]

[1]DPRI, Kyoto University, Uji, Japan

[2]Laurence Livermore National Laboratory, Livermore, CA, USA

E-mail contact of main author: kawase@zeisei.dpri.kyoto-u.ac.jp

Abstract. For the quantitative simulation of strong motions we have been using intensively a kinematic source models with a complex prescription of slip along the fault surface. In these years we have been developing dynamic rupture simulation techniques based on the nonlinear constitutive law on the fault surface. We investigate the effects of source parameters that describe the complex nature of the source process. The important ingredient here on the stress distribution on the fault is the asperity (or asperities) with the characteristic size controlled by the scaling low with respect to the entire rupture areas. We construct the initial boundary conditions based on such a scaling low about the major asperity (or asperities), together with the random perturbation of stress drop distribution on the fault. We also consider the depth dependence of the S-wave velocity, the slip-weakening distance Dc, and the background average stress drops. Geometric parameters such as the rupture initiation point, relative separation distance between two asperities, and the depths of the two asperities are also chosen to investigate. The assumed fault is the vertical strike-slip fault with the size corresponding to M6.7. It is quite interesting to see the strong effect of Dc, asperity depths, and the average stress drop distribution. If we put asperities in the deeper part of the fault, we could not see much of the surface rupture. If we put two asperities close enough, the resultant slip distribution would be larger not only in depth but also on the surface. If we increase Dc slightly, then the resultant slip tends to be smaller and smaller, and finally the rupture will be trapped in the middle of the rupture propagation. If we assume very small amount of stress drop near the surface, we do not see large surface slip in the end.

Key Words: Dynamic rupture, Slip distribution, Stress drop, Slip weakening.

1. Introduction

From the latter half of the 1970s, the dynamic rupture simulation of fault motions has been investigated based on the fracture mechanics, starting from simple fracture problems of cracks. The initial researches were focused on reproducing the basic dynamic rupture properties, such as whether or not the rupture progresses, how the propagation speed changes when it progresses, and what is the shape of the slip velocity function in asperities, by setting the fracture parameters on simple and uniform fault rupture surfaces. Thereafter, it has been found that the nonlinear fracture behaviour of the fault plane can be clearly described by a slip-weakening model, and the model can reproduce recorded near-fault ground motion characteristics. In particular, with the increase of the speed and the scale of computers, realistic rupture simulations have become possible by setting heterogeneous fault rupture parameters considering both the depth dependency and random fluctuations, instead of the spatial distribution of a homogeneous fault rupture parameter.

There is a limit for the amount of data available for deriving important empirical relationships, such as the relationship between the fault width and seismogenic layer, the relationship between the maximum and average slips in the seismogenic layer and at the ground surface, and the influence of coupling of asperities on slip, for predicting strong ground motion only by analysing observed data of past earthquakes. On the other hand, through numerical simulations of fault rupture dynamics, it is possible to obtain important information on the type of final slip distribution that can occur in a stress state before the occurrence of multiple earthquakes by performing parametric analysis on specific relationships. However, the range of fault rupture parameters to be used in the parametric studies should be physically valid.

As a joint research between LLNL and DPRI on the rupture dynamic rupture dynamics for crustal earthquakes, we carried out analyses on the effects of several dynamic rupture parameters, such as stress drop, slip weakening distance, and stress excess on fault rupture slip, slip velocity, and rupture speed. In addition, we examined potential relationships between the assumed initial stress conditions, including asperities location, and rupture initiation time and the final slip and slip velocity obtained from the spontaneous rupture modelling.

2. Method of simulation

Here, we describe the basic features of the finite-difference method for modelling the rupture dynamics used in Pitarka et al. (2009) [1], which is based on the method proposed by Dalguer and Day (2007) [2].

In the formulation of Dalguer and Day (2007) [2], two nodes are placed at the same position on the fault plane, and the continuity conditions of the equilibrium of forces and displacement between the two points are considered. The differential scheme involves a staggered grid finite difference method for velocity and stress. The setting of shear stress on the fault plane is carried out according to the following equation.

$$\tau_c - \tau \geq 0 \tag{1}$$

$$\tau_c \dot{\mathbf{s}} - \boldsymbol{\tau} \dot{s} = 0. \tag{2}$$

Here, τ is the shear stress acting on the fault plane, s is the displacement vector, and c represents the shear strength of the plane. Equation (2) shows the equilibrium of out-of-plane forces. The equation of motion of the fault plane is expressed as below.

$$\rho_{j,k}^{\pm}\left\{\frac{\left[\dot{u}_x^{\pm}(t+\Delta t/2)\right]_{j,k}-\left[\dot{u}_x^{\pm}(t-\Delta t/2)\right]_{j,k}}{\Delta t}\right\}$$

$$=\frac{\left[D_x^{(2)}\sigma_{xx}^{\pm}(t)\right]_{j,k}+\left[D_y^{(2)}\sigma_{xy}^{\pm}(t)\right]_{j,k}\pm 2\left\{\left[\sigma_{xz}(t)\right]_{j,k,l_0\pm 1/2}-\left[T_x(t)-T_x^0\right]_{j,k}\right\}}{\Delta x}, \tag{3}$$

Here, the left-hand side is the acceleration times the mean density at time t at point (j, k), and the right-hand side is the spatial derivative of the stress on the fault plane. T is the shear traction

on the fault plane, and T0 is the initial value. D_i is the differential operator. By solving this equation with the finite difference method, the amount of slip on the fault plane is obtained.

As a constitutive relationship at the fault surface in the studies of Dalguer and May (2007) [2] and Pitarka et al. (2009) [1], the simple slip weakening model of Andrew (1976) [3] is used, which is shown in Fig. 1. The symbols used here are:

σ_u : maximum stress (strength)

σ_0 : initial stress

σ_r : residual stress

T_u : breakdown stress drop

T_e : dynamic stress drop

D_c : critical slip weakening distance

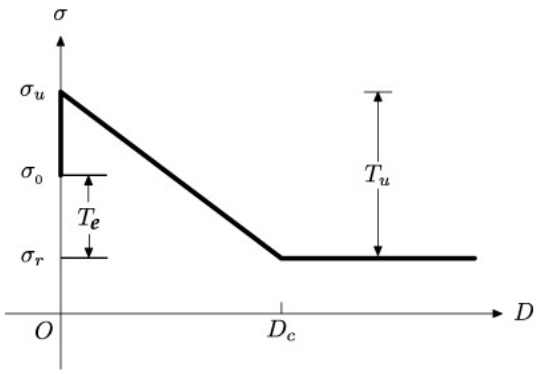

Fig. 1. Slip-weakening model (Andrew, 1976) used in the study.

The advantage of using a linear slip weakening friction law is that the modeller can directly impose the expected amounts of stress drop and strength excess out of the spontaneous rupture model, without necessarily using absolute values of the initial normal and shear stresses as inputs. Dalguer and May (2007) [2] compared the resulting time histories of the stress and slip velocity functions at the two points on the fault plane for two different grid sizes (namely 100m and 300m) with the conventional method, which was calculated using 50 m grid. Although there is a difference between the results of the 300 m grid-size case and that of the conventional method, there is almost no difference between the results of the 100 m grid-size case and that of the conventional method.

Then by using spontaneous rupture simulations for M6.9-7.3 crustal earthquakes, Pitarka et al. (2009) [1] examined how the frequency content of computed strong motion characteristics depends on whether the rupture crosses the entire weak zone and reaches the free surface. In their stress model the stress drop on the fault plane and shear and normal stresses were spatially varied using a stochastic scheme. The spatial variation of stress drop follows the k^{-2} model of Mai and Beroza (2002) [4] derived from analysis of empirical data of spatial slip distributions. The average stress drop is set to 5 MPa, and the amount of stress drop near the surface as well as the bottom is reduced so that the amount of slip gradually decreases in the upper 5 km of the top of the fault rupture and the bottom 3 km of the fault below 15 km. The value of the critical slip weakening distance Dc is gradually increased in both top and bottom parts of the fault.

In Pitarka et al. (2009) [1] three different stress drop distributions were considered in which the reduction rate of stress drop in the shallow portion of the fault is varied in order to produce three distinct rupture scenarios. In the first scenario with a gentle reduction rate the fault rupture reaches the surface, and the resulting ground displacement is substantial. In the second scenario with a moderate reduction rate the rupture reaches the surface but the resulting ground displacement is very small. In the third scenario with zero stress drop near the surface, representing buried fault earthquakes, the rupture does not reach the free surface. The effects of weak zone on rupture dynamics, as well as shallow slip and near-fault ground motion are quite significant. The peak ground motion velocity is higher for buried ruptures and lower when rupture reaches the free surface. This correlation is reversed for the near-fault ground motion displacement and long period ground motion velocity.

By referring to these previous studies we conducted parametric studies focusing on the dynamic fault parameters, especially the depth dependence of them, to delineate their influence on the slip distribution on the fault surface and the resulting ground velocity levels. The major difference of our simulation to the previous studies is that we introduce a couple of rectangular high-stress drop patches that correspond to the asperities delineated from the kinematic rupture process inversions (Irikura and Miyake, 2002 [5]).

3. Results of Parametric Studies

3.1. Models of the parametric analyses

In our analysis of the effects of dynamic rupture parameters on simulated rupture kinematics and near-fault ground motions we focused on the following rupture model parameters:

- the asperity depth

- the rupture initiation point

- the slip weakening distance, Dc

- the gradient that controls the stress drop near the ground surface.

The fault model used is an inland crustal earthquake equivalent to M6.7 with a maximum length of 25 km and a maximum width of 18 km, as a vertical strike-slip fault. Table 1 shows the one-dimensional ground structure used in the model. We assume a shallow bedrock structure of 5 km depth under a soft rock layer of 1 km thickness. We also assume a homogeneous half space below 5 km.

Table 1. One-dimensional crustal structure used in the simulation.

Layer	Depth(km)	Vp(km/s)	Vs(km/s)	density
1	0.5	1.2	0.68	2.1
2	1	1.9	1	2.2
3	5	4.8	2.8	2.4
4	Half Space	6	3.464	2.67

3.2. Effects of asperity depth

Here we investigate the effects of asperity depth on computed final slip distribution. We used Irikura Recipe [5] for strong ground motion simulations to estimate the number and size of asperities (i.e., a patch with elevated stress drop) expected for a M6.7 crustal earthquake. According to the recipe the number of asperities for a M6.7 earthquake should be two. Figure 2 shows the dynamic fault rupture parameters used in rupture scenarios of Case 1, in which one deep asperity and one shallow asperity were included, and Case 2, in which both asperities are shallow. The top left, top right, middle left, middle right and the bottom left of each figure show the shear stress, normal stress, and stress drop, strength excess distributions, and critical slip-weakening distance Dc, respectively. Except for Dc, random spatial variations of stress parameters were imposed simultaneously. The random spatial variation follows the k^2 model of Mai and Beroza (2002) [4], as used in Graves and Pitarka (2010) [6].

Figure 3 shows the comparison of computed final slip, spontaneous rupture time, and assumed stress drop between deep (Case 1) and shallow (Case2) asperities rupture scenarios. As seen in this figure, when one of the asperities is deep, the resulting slip distribution follows the asperity locations. In contrast, when both asperities are shallow, because of the rupture interaction with the free surface, the resulting slip is more homogeneous and unfirmly distributed in the asperity areas. The deep asperity does not contribute so much to the near-surface slip.

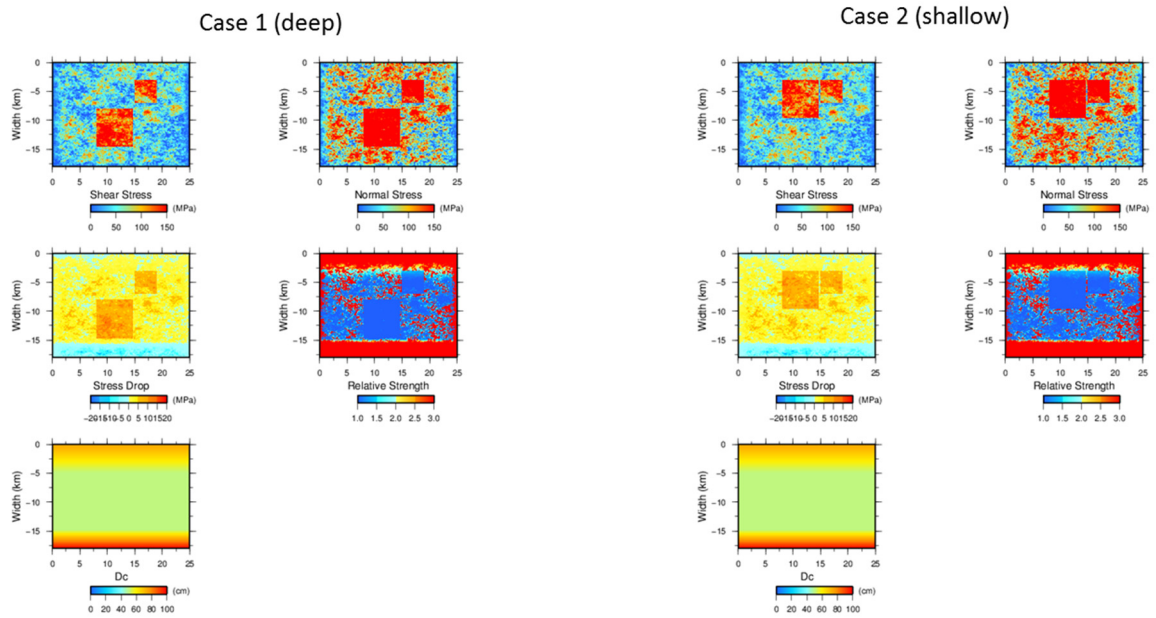

Figure 2. Parameters for deep (Case 1) and shallow (Case 2) asperity scenarios.

Next, we generated a suite of 120 rupture realizations for which the small asperity remained fixed in its original position, as shown in Figure 2, while the large asperity was randomly located at different depths starting from shallow (2-6 km), intermediate (6-8km) to deep (8-10 km). The result of the simulations in terms of maximum and average slip, and maximum and average ground motion surface velocity is shown in Figure 4. It is important to note that the average slip is remarkably constant with a slight tendency to decrease with the asperity depth. The same tendency with a larger variation is observed in the maximum slip. The mean and maximum ground surface velocity follows similar trend. However, the decrease in the maximum and average velocities with respect to the asperity depth is more than a factor of two, as opposed to only 25% decrease seen in the maximum slip.

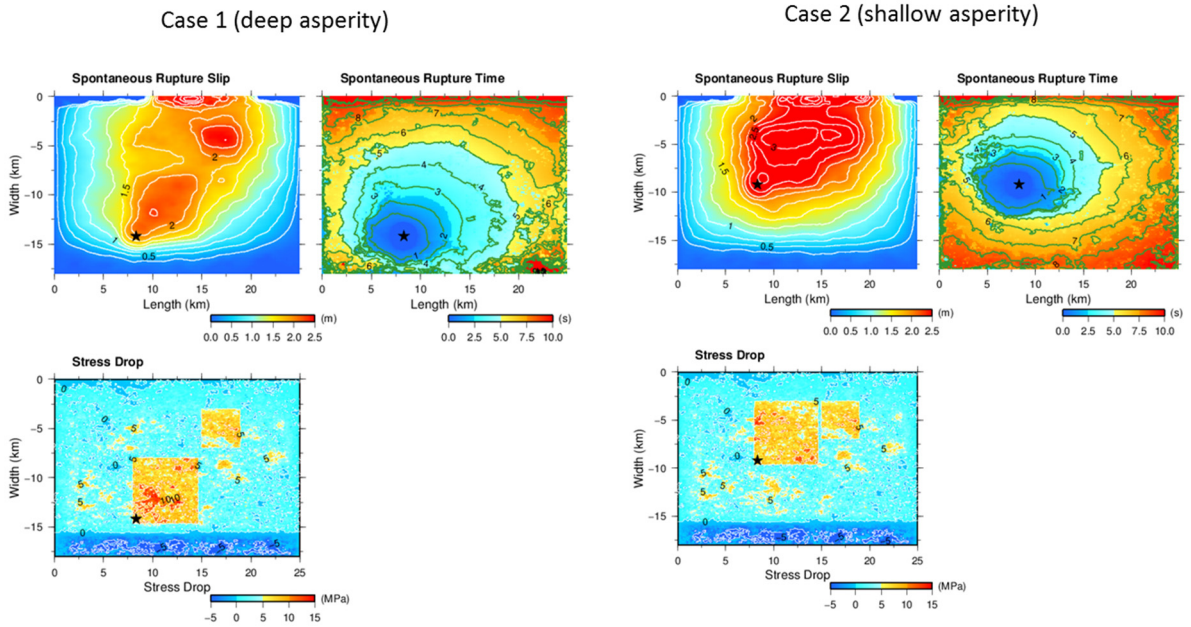

Figure 3. Comparison of slip amount and rupture initiation time between deep and shallow asperity scenarios.

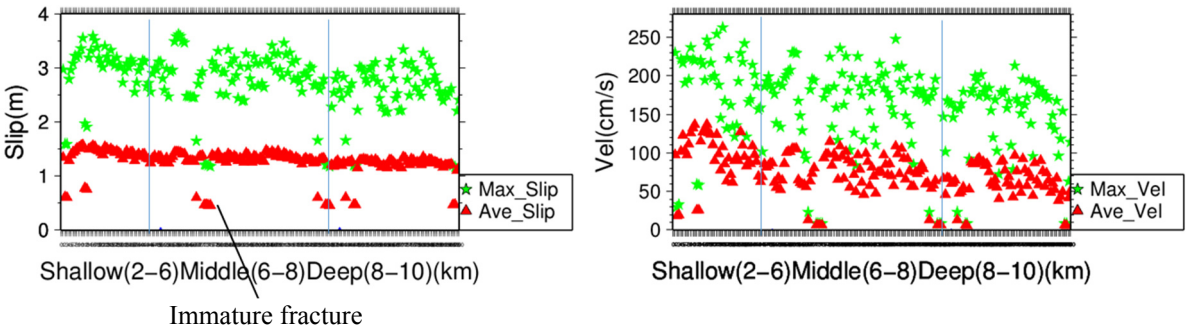

Figure 4. Fluctuations in the slip amount and ground velocity by changes in the larger asperity depths.

3.3. Effects of the distance between asperities

Here we investigate the effects of inter-asperities distance on simulated final slip and near-fault surface ground motion velocity. Figure 5 shows the dynamic fault rupture parameters for the rupture scenario Case 1, in which the small and large asperities are located next to each other, and Case 2 in which the asperities are separated by 4 km. The resulting distributions of final slip, spontaneous rupture time, and assumed stress drop are shown in Figure 5 as before.

The two asperities in close proximity to each other in Case 1 act as a single asperity. The corresponding large slip area is larger than the large slip area obtained for Case 2 where the asperities are well separated. Most importantly, the second model produces smaller fault surface slip and subsequent ground velocity.

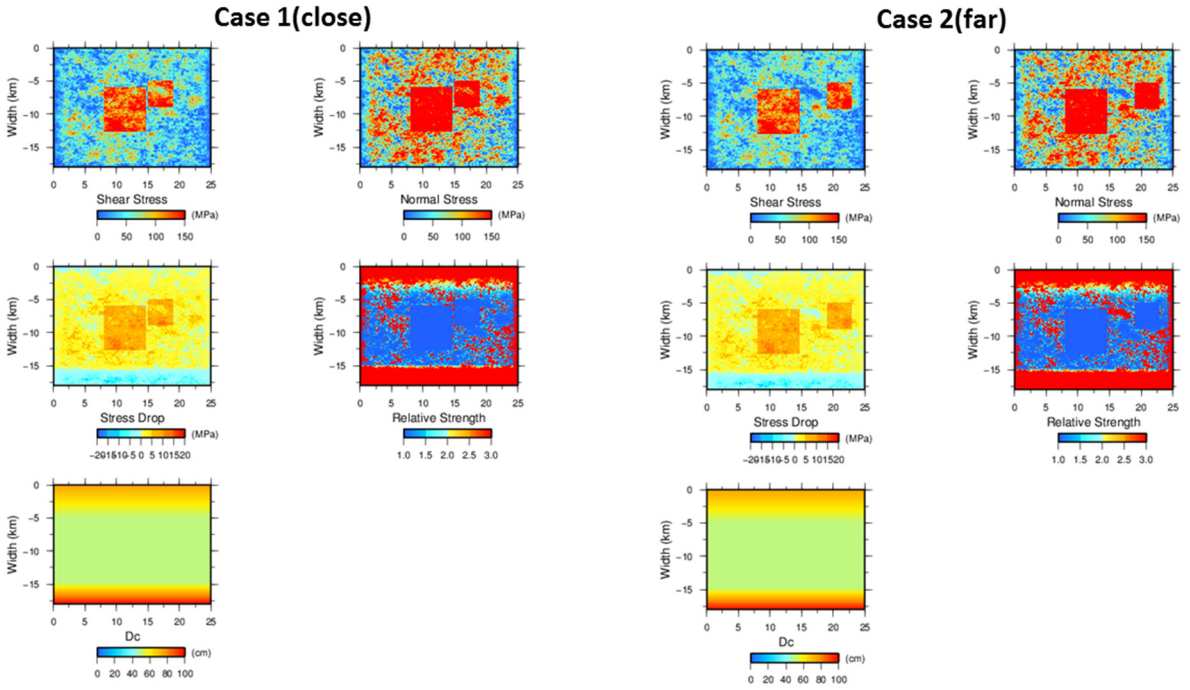

Figure 4. Parameters for close asperity scenario (Case 1) and far asperity scenario (Case 2).

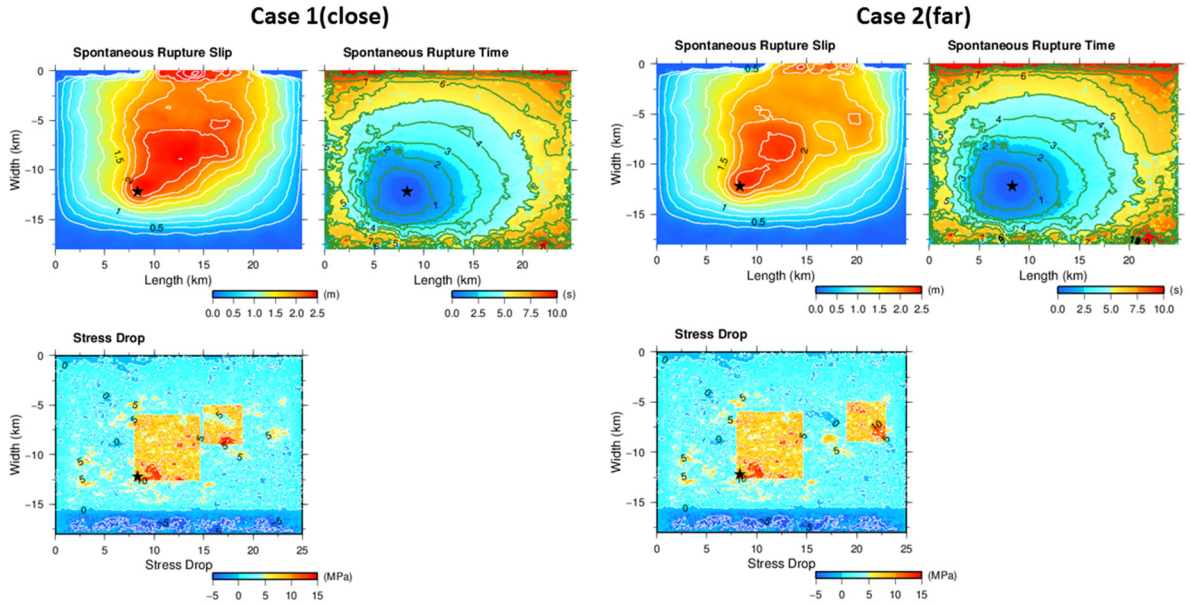

Figure 5. Resultant effects of asperity distance on slip distribution and rupture initiation time.

Figure 6 shows variations of computed fault slip and near-fault surface ground motion velocity as a function of the inter-asperity distance. We use 120 rupture scenarios for which the inter-asperity distance randomly varies between 0 to 4.7 km. We should note that the average slip is practically independent of the inter-asperity distance. This could be due to the fact that in all 120 scenarios the separation between the asperities is relatively small compared to the size of the largest asperity. On the other hand ground motion velocity is sensitive to the inter-asperity distance, and varies by more than a factor of two between the scenarios. Being representative of higher frequency ground motion the near-fault peak velocity is sensitive to the local directivity effects and interactions between the local rupture dynamics and the free surface.

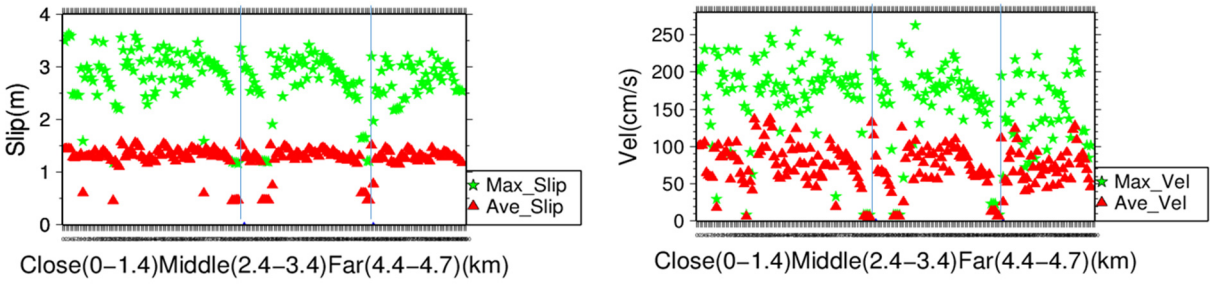

Figure 6. Fluctuation ranges of slip and ground surface velocity due to changes in inter-asperity distance.

3.4. Effects of rapture initiation point

In all the rupture scenarios described above the rupture initiates in the lower left corner of the large asperity. This particular locations favors upward directivity effects and in the case of shallow asperities favors along strike directivity effects, too. The rupture initiation location should have significant impact on the overall spontaneous rupture process. We investigated its influence on the results of slip and ground velocity. Figure 7 illustrate two rupture scenarios with identical parameters except for the rupture initiation location. In Case 1 the rupture starts from the lower corner, while in Case 2 it starts from the upper corner of the large asperity.

The slip and rupture time distributions resulting from each scenario are shown in Figure 8. There is a significant difference in slip and rupture time distributions between the two scenarios. It is obvious that rupture initiation controls effects of local rupture directivity.

As indicated by the simulation results shown in Figure 9, there is a large variation in both slip

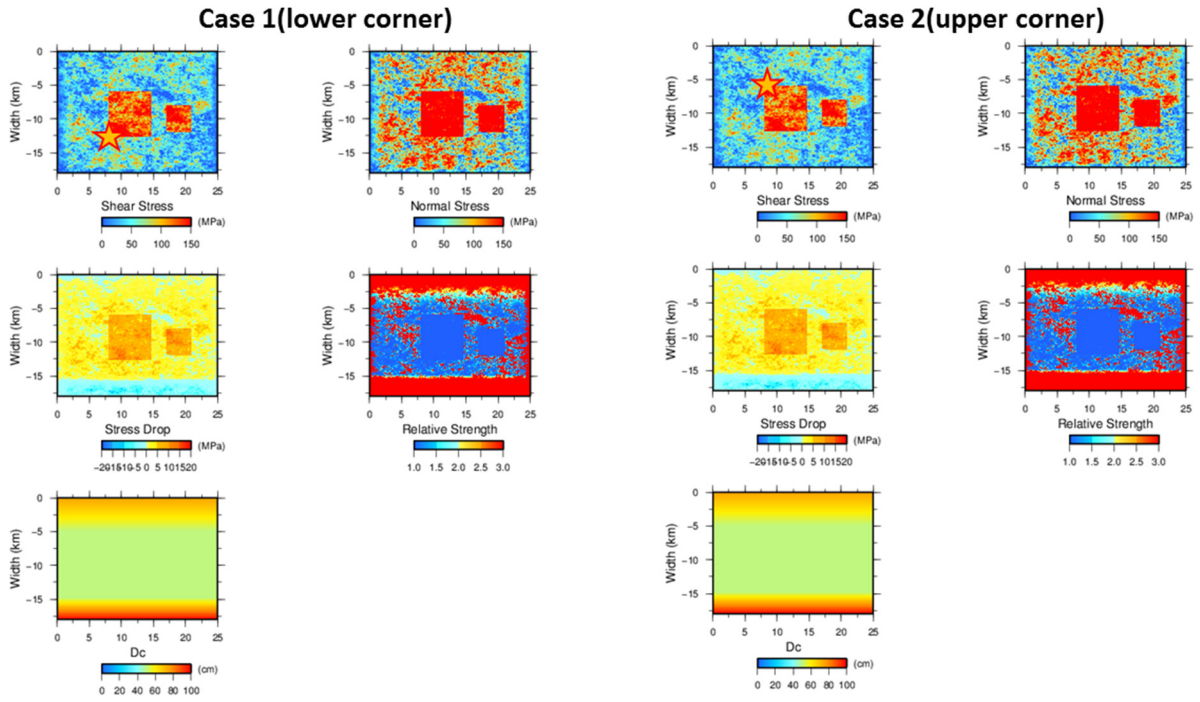

Figure 7. Deep initiation point (☆) scenario (Case 1) and shallow initiation point scenario (Case 2).

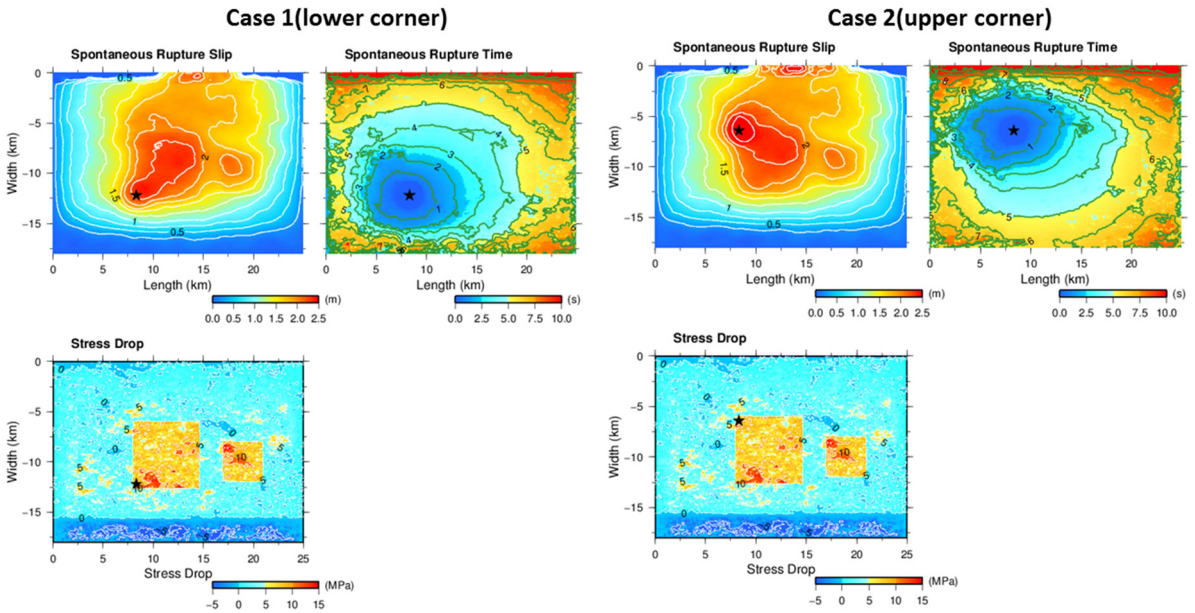

Figure 8. Effects of the rapture initiation point on slip distribution and rupture initiation time.

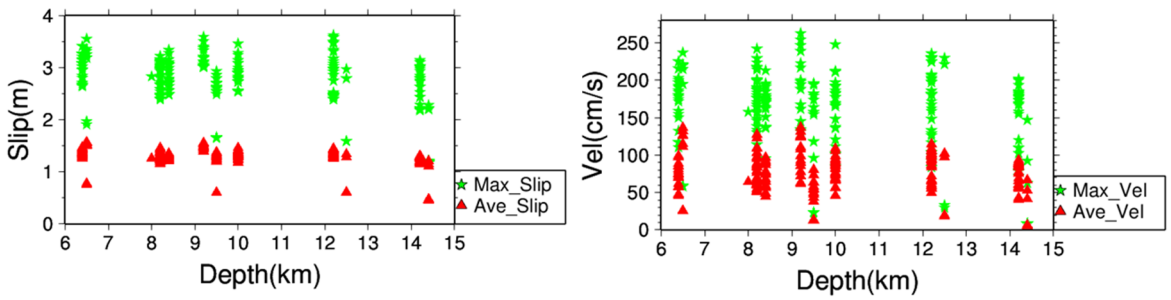

Figure 9. Fluctuation ranges of slip and ground surface velocity by the depth variations of the rapture initiation points.

and peak ground motion velocity. The variability does not necessarily correlates with rupture initiation depth, since the effect of rupture directivity as well as spontaneous rupture propagation speed depends on relative location of asperity areas with respect to the rupture initiation location and proximity to the free surface.

3.5. Effects of Dc

The critical slip-weakening distance D_c controls the fracture energy. A larger D_c increases the energy consumed by the fracture. Consequently a larger Dc suppresses the advancement of fracture because a larger energy is required by the fracture to propagate. Relatively speaking, large Dc slows down the rupture, while small Dc increases the rupture propagation speed, and consequently increases the slip velocity. Since Dc trades off with stress drop, its effect on rupture propagation also depends on the assumed overall stress distribution on the fault. In our rupture models the Dc is set to 50 cm in the seismogenic zone (depths range 5-15km) and it linearly increases at depths shallower than 5km and deeper than 15km. The Dc at the ground surface is set to 75 cm, and 100 cm at 18km. We investigated the effects of Dc assigned to the seismogenic zone on rupture dynamics by performing simulations with three different models with different Dc, Case 1, Case2, Case3, for which Dc are 50cm, 52cm and 55cm, respectively. Figure 10 shows the stress models, and Figure 11 shows the results of rupture

dynamics simulations. In Case 3 where Dc=55 cm the rupture stops as soon as it starts. Decreasing Dc from 52cm to 50 cm increases the rupture speed and slightly increases the free surface slip. Based on the similar analysis of Dc, most of our stress models have a Dc with a base value of 50 cm which produces a sub-shear rupture propagation.

Figure 12 shows time histories of ground motion surface velocity computed at a linear array of

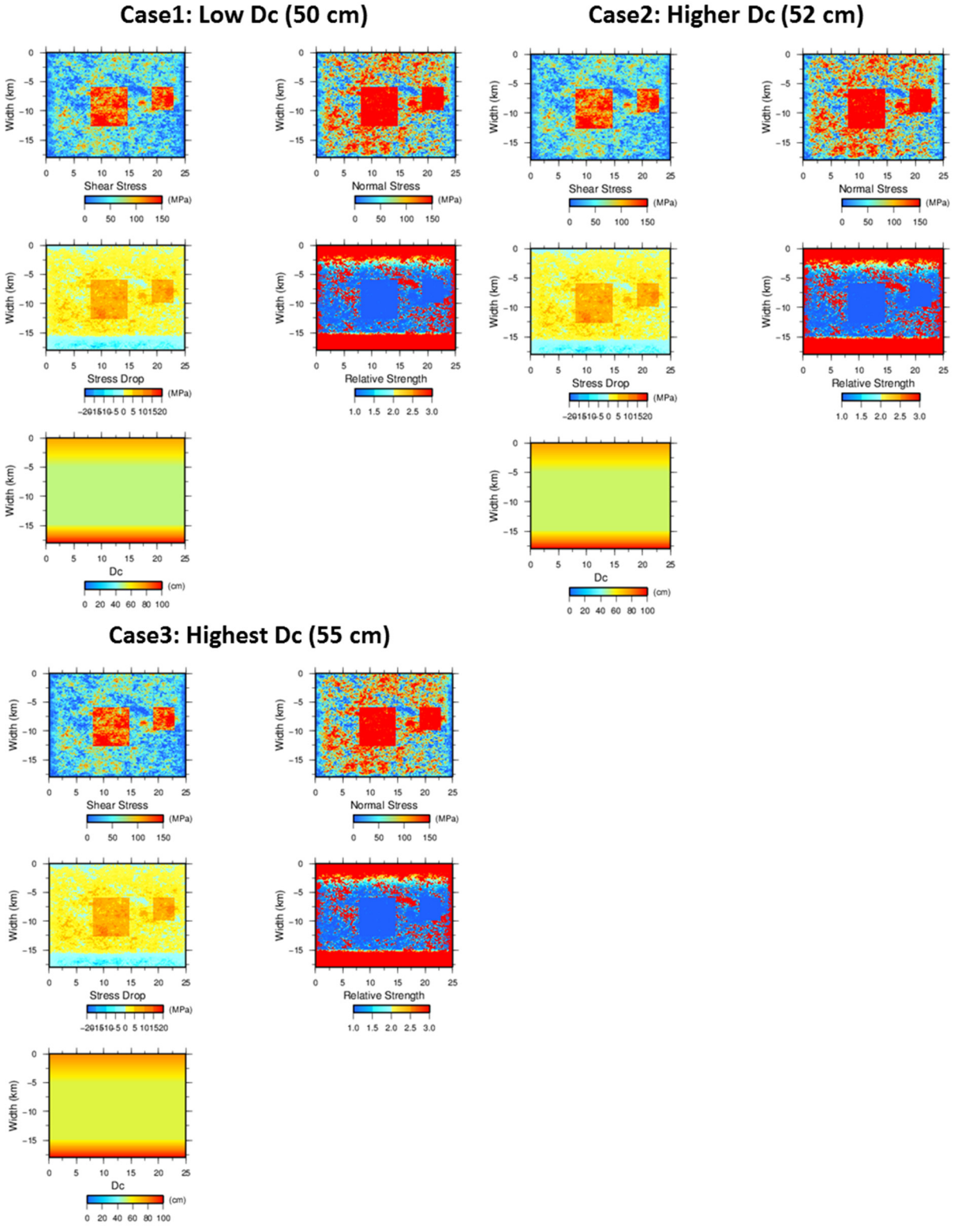

Figure 10. Source parameters of small Dc (Case 1), slightly larger Dc (Case 2), and large Dc (Case 3).

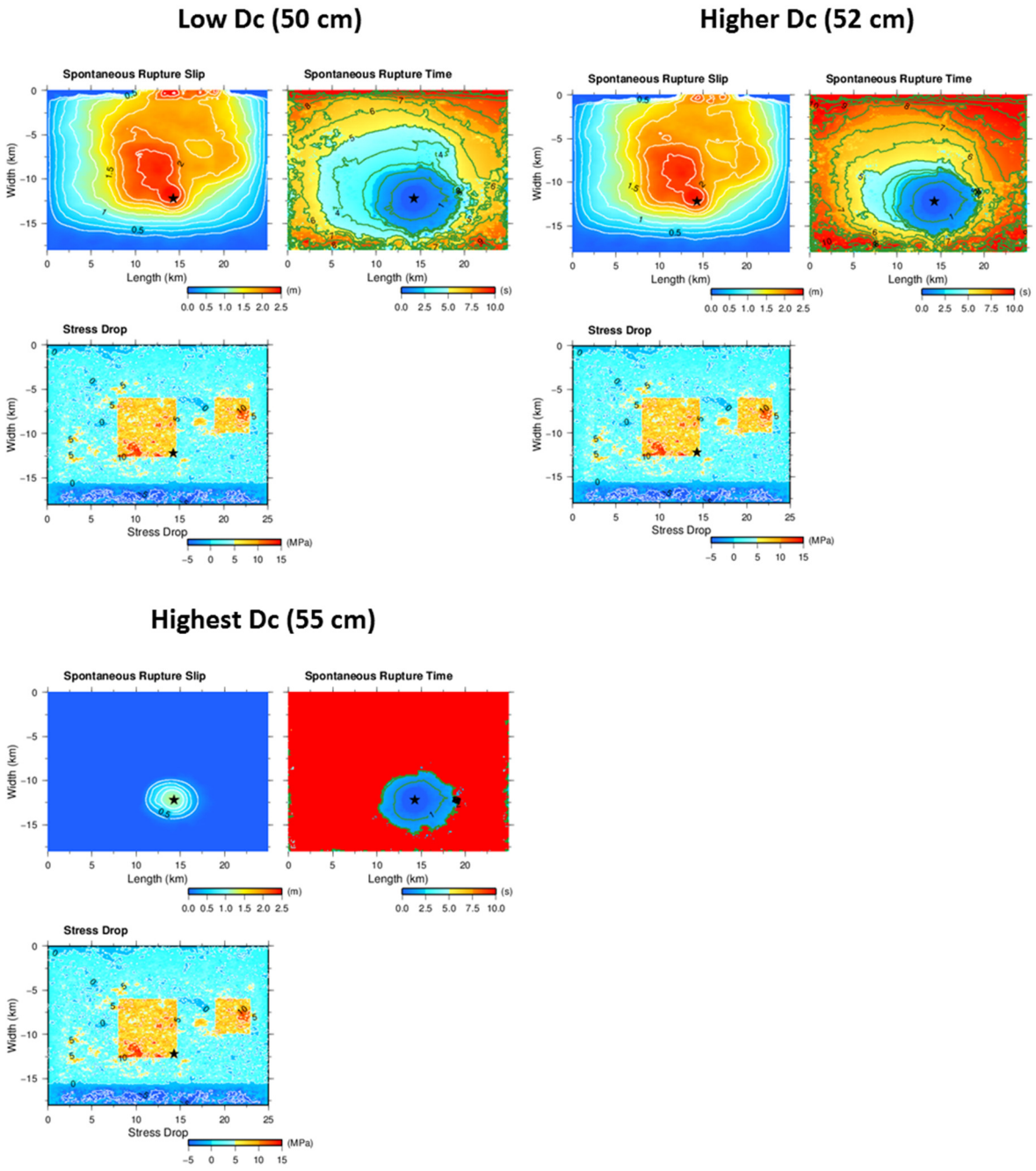

Figure 11. Comparison of slip and rapture initiation time for three cases with different Dc values.

13 receivers located 200m east of the fault trace, for Case 1 (Dc=50cm) and Case 2 (Dc=52cm). The NS component is a perpendicular to the fault, and EW component is parallel to the fault. The fault normal component exhibits clear rupture directivity effects on ground motion peak amplitude. A smaller Dc causes the rupture speed and peak slip velocity to increase. Consequently the ground motion for Case 1 is larger than that of Case 2.

When we see the results of simulation for cases with Dc values from 50 cm to 55 cm in every 1 cm interval, we found that the rupture process is quite sensitive to the assumed value of Dc, as only 1 cm increase makes difference between the whole surface rupture and the immature rupture termination with exactly the same stress drop settings.

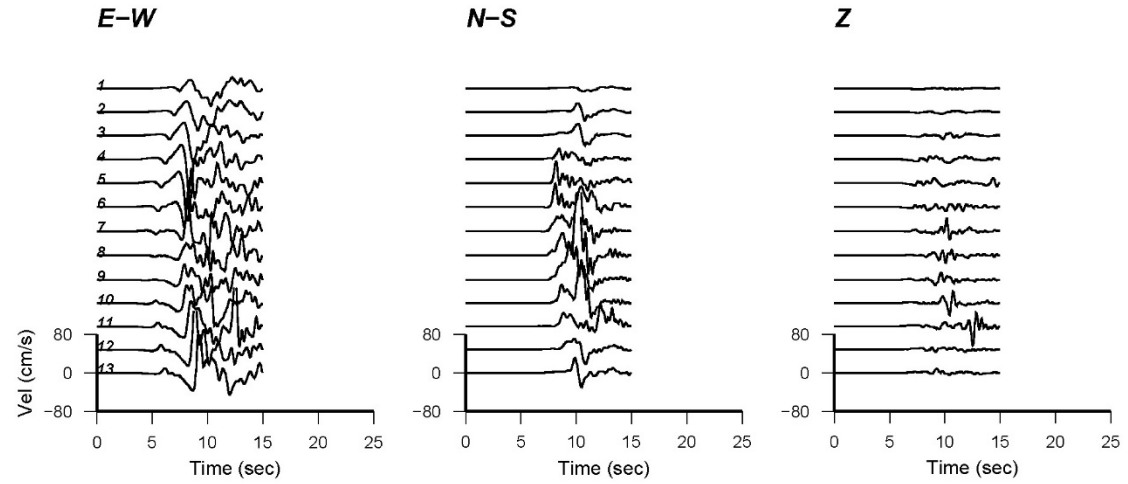

(a) Dc=50cm

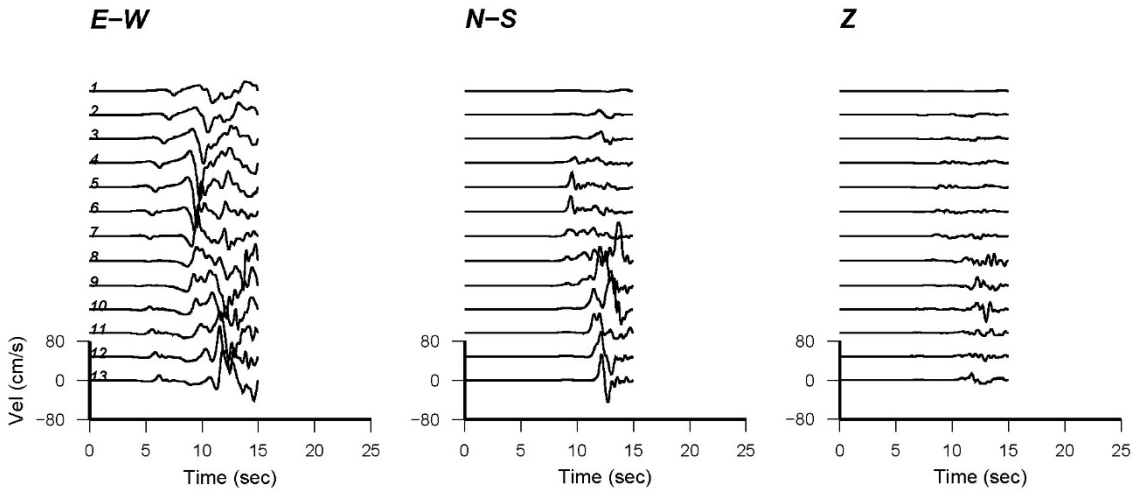

(b) Dc=52cm

Figure 12. Ground surface velocity distribution along the fault strike direction for Dc=50cm and Dc=52cm.

3.6. Effects of stress drop near the surface

Here we investigate the effect of near surface stress drop on simulated rupture dynamics and near-fault ground motion. As explained earlier, we included a weak zone in which stress drop is set to zero or negative at the free surface and linearly increases with depth in the top 5 km of the crust. In this study the average stress drop at 5km depth was set to 3.2 MPa. We considered two stress models. In Case 1 model, the near-surface stress-drop gradient is 0.06MPa/km which yields a zero stress drop at the free surface. In Case 2 model, the gradient was 0.064MPa/km which yield a negative stress drop at the free surface (Figure 13).

Figure 14 shows the simulated final slip and rupture time distributions for Case 1 and Case 2 models. The slip distribution shows that the near-surface slip is very sensitive to the stress drop in the shallow part of the crust. A weaker near-surface zone (smaller stress drop zone with large Dc) limits the surface rupture to a smaller portion of the fault. When we see the maximum and average slip, and maximum and average ground motion velocity for several cases with different stress drop gradient to the surface, we found that the maximum slip (concentrated along the free

surface) decreases with decreasing near-surface stress drop. The effect is drastic on ground motion amplitudes; peak velocity increases by a factor of 3 when near-surface stress drop increases from a negative value to zero.

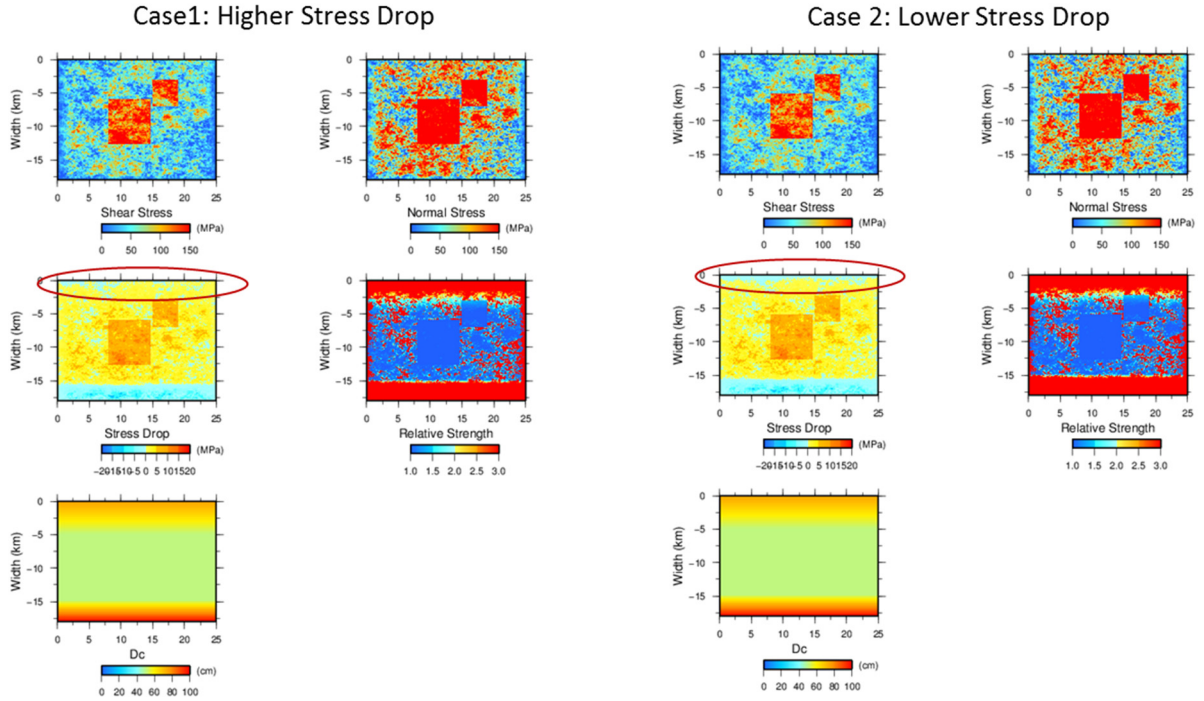

Figure 13. Case where stress drop near the surface is almost zero (Case 1), and case where it is a negative value (Case 2)

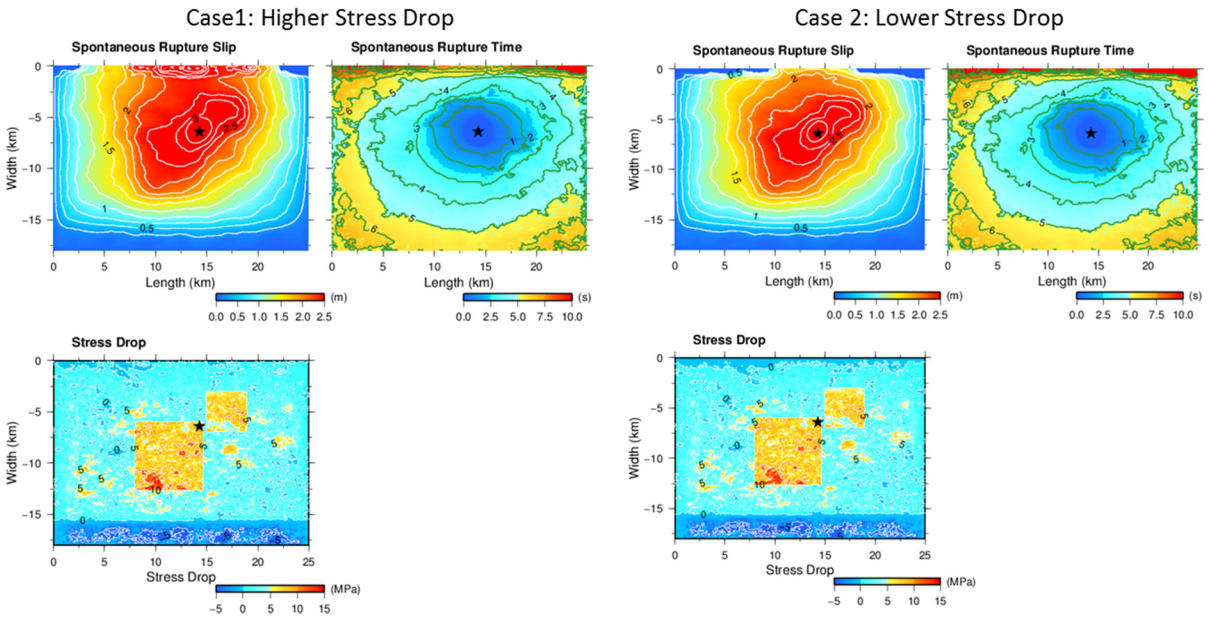

Figure 14. Comparison of slip and rapture initiation time between two cases of different stress drop near the surface.

4. Summary and Conclusions

In our analysis of effects of dynamic rupture parameters on simulated rupture dynamics and near-fault ground motion we focused on the following rupture model parameters:

- the asperity depth
- the inter-asperity distance
- the rupture initiation point
- the slip weakening distance, D_c, and
- the near-surface stress drop.

The conclusions drawn from the numerical experiments are:

1) *Effects of asperity depth*:

Shallower asperities generate larger mean and maximum fault slip, as well as larger near-fault ground motion velocity. The mean and maximum ground surface velocity follow similar trends. However, the decrease in maximum peak and average velocities with asperity depth is more than a factor of two, as opposed to only 25% decrease in maximum slip.

2) *Effects of inter-asperity distance*:

The average slip is practically independent of the inter-asperity distance. This could be due to the fact that in all scenarios considered here the separation between the asperities is relatively small compared to the size of the largest asperity. On the other hand ground motion velocity is sensitive to the inter-asperity distance (local cumulative rupture directivity), and varies by more than a factor of two between the scenarios. Being affected by high frequency ground motion the near-fault peak ground motion velocity is sensitive to the local directivity effects and local interactions between local rupture dynamics and the free surface.

3) *Effects of location of rupture initiation point*:

Rupture initiation location controls local rupture directivity. As indicated by the simulation results shown in Figure 9, there is a large variation in both slip and peak ground motion velocity. The variability does not necessarily correlates with rupture initiation depth, since the effect of rupture directivity as well as spontaneous rupture propagation speed depends on relative location of asperity areas with respect to the rupture initiation location and proximity to the free surface.

4) *Effects of critical slip-weakening distance Dc*:

It was found that critical slip-weakening distance Dc has little effect on mean and maximum slip amounts. However, if Dc is too large, it causes immature fracture, while large Dc results in small mean and maximum ground surface velocity.

5) *Effects of near-surface stress drop*:

The slip distribution shows that the near-surface slip is very sensitive to the stress drop in the shallow part of the crust. A weaker near-surface zone (smaller stress drop and large Dc) limits the surface rupture to a smaller portion of the fault. We found that the maximum slip (concentrated along the free surface) decreases with decreasing near-surface stress drop. The effect is drastic on ground motion amplitudes. Peak velocity increases by a factor of 3 when near-surface stress drop increases from a negative value to zero.

Based on these results, the following investigations are necessary in future researches:

· To perform calculations for uniform and semi-infinite ground, which means that we assume no low velocity layers near the ground surface. A soft material near the surface used here is likely to have significant effects.

· To perform calculations for earthquake with larger magnitude because this study investigated only cases of intermediate-size earthquake of M6.7.

· To investigate how much effects will be manifested when the dependency of stress drop with depth (e.g., Nakano et al., 2015 [7]) in the seismogenic zone is considered.

· To examine whether the scaling law of asperity [5], derived by characterizing the obtained slip distributions from the method for kinematic inversions, agrees with that from the dynamic rupture simulations.

· To obtain the ground motion prediction equation (GMPE) from simulated velocity waveforms and compare it with the empirical GMPEs.

REFERENCES

[1] PITARKA, A., L.A. DALGUER, S.M. DAY, P.G. SOMERVILLE, and K. DAN. "Numerical Study of Ground-Motion Differences between Buried-Rupturing and Surface-Rupturing Earthquakes", Bull. Seismo. Soc. Am., Vol. 99, No. 3, 1521-1537, doi: 10.1785/0120080193 (2009).

[2] DALGUER, L. A., and S. M. DAY. "Staggered-grid split nodes method for spontaneous rupture simulation", J. Geophys. Res. 112, B02302, doi 10.1029/2006JB004467 (2007).

[3] ANDREWS, D.J., "Rupture velocity of plane-strain shear cracks", J. Geophys. Res. 81, 5679-5687 (1976).

[4] MAI, P. M., and G. C. BEROZA. "A spatial random field model to characterize complexity in earthquake slip", J. Geophys. Res. 107, no. B11, 2308, doi 10.1029/2001JB000588 (2002).

[5] IRIKURA, K. and H. MIYAKE. "Recipe for predicting strong ground motion from crustal earthquake scenarios", Pure Appl. Geophys., 168, 85-104, doi:10.1007/s00024-010-0150-9 (2011).

[6] GRAVES, R. W., and A. PITARKA. "Broadband ground-motion simulation using a hybrid approach", Bull. Seismol. Soc. Am. 100, no. 5A, 2095-2123, doi: 10.1785/0120100057 (2010).

[7] NAKANO, K., S. MATSUSHIMA, and H. KAWASE, "Statistical properties of strong ground motions from the generalized spectral inversion of data observed by K-NET, KiK-net, and the JMA Shindokei Network in Japan", Bull. Seismo. Soc. Am., Vol.105, 2662-2680, doi:10.1785/0120140349 (2015).